

Two-dimensional ferromagnetic ordering and magnetoresistance in the layered perovskite $\text{La}_{2-2x}\text{Ca}_{1+2x}\text{Mn}_2\text{O}_7$

H. Asano, J. Hayakawa, and M. Matsui

Department of Materials Science and Engineering, Nagoya University, Furo-cho, Chikusa-ku, Nagoya, 464-01, Japan

(Received 4 March 1997)

The resistivity and magnetization of layered perovskite $\text{La}_{2-2x}\text{Ca}_{1+2x}\text{Mn}_2\text{O}_7$ have been studied systematically using bulk samples with a wide doping concentration range $0 \leq x \leq 0.5$ and epitaxial thin film samples with $x=0.3$. The system becomes a metallic ferromagnet for doping concentrations $0.22 \leq x \leq 0.5$. In this doping region, results for bulk samples as well as for thin films have clearly shown that there are two types of ferromagnetic ordering, possibly originating from an anisotropic exchange interaction. Magnetoresistance is observed over a wide temperature range below the ferromagnetic ordering temperatures. Based on these results, a model of temperature-dependent spin ordering is presented for a double perovskite ferromagnet, which suggests that there is a two-dimensional ferromagnetic alignment at temperatures between the two ordering temperatures. [S0163-1829(97)03433-4]

I. INTRODUCTION

Since the discovery of high-temperature superconductivity in perovskite copper oxides, there has been revived interest in mixed-valence manganese perovskites. The colossal magnetoresistance (CMR) effect in doped manganese perovskites has attracted great attention with regard to scientific study and technological applications. The cubic (or pseudocubic) perovskites $R_{1-x}M_x\text{MnO}_3$ (R being rare-earth ions and M divalent cations), such as $\text{La}_{1-x}\text{Ca}_x\text{MnO}_3$ and $\text{La}_{1-x}\text{Sr}_x\text{MnO}_3$, with three-dimensional Mn-O networks (isotropic MnO_6 octahedra), are known to become conducting ferromagnets at hole doping concentrations of $x > 0.2$ and exhibit CMR effects.¹⁻⁹ The magnetic and electronic properties have been examined within the framework of the double-exchange theory, which considers the transfer of an electron between neighboring Mn^{3+} and Mn^{4+} ions the Mn-O-Mn path.¹⁰⁻¹² Under the circumstance of the octahedral symmetry of the Mn sites, the electron configuration becomes $t_{2g}^3 e_g^1$ for Mn^{3+} and t_{2g}^3 for Mn^{4+} . The e_g^1 electrons can be treated as mobile charge carriers which interact, due to the strong Hund exchange coupling, with the localized t_{2g}^3 electrons ($S = \frac{3}{2}$). The electron transfer depends on the relative alignment of the local spins. Thus, the model, which is based on the effective exchange coupling induced by carrier transfer (hopping), can describe important aspects of both the magnetic and transport behavior in manganites. The negative magnetoresistance in the perovskite manganites can be interpreted in terms of increased carrier hopping induced by the spin alignment in an applied magnetic field. However, recent theoretical and experimental studies¹³⁻¹⁸ have suggested that, in addition to the double-exchange theory (spin-dependent electron hopping mechanism), some other effects, such as those relating to static or dynamic lattice distortions of the MnO_6 octahedra, are needed to enable us to understand the interplay between the carrier transport and spin arrangement and the mechanism producing the CMR effect.

Systematic studies have provided the phase diagrams^{8,19} of temperature versus doping concentration for the cubic (or

pseudocubic) perovskites, such as $\text{La}_{1-x}\text{Ca}_x\text{MnO}_3$. In a system with appropriate doping ($x \sim 0.3$), a ferromagnetic metal (FM) to paramagnetic insulator (PI) transition takes place at the magnetic transition temperature T_c . The temperature and carrier doping driven metal-insulator transition is associated with this magnetic transition temperature, around which CMR effects have been observed. Thus, the temperature for the maximum magnetoresistance correlates well with the peak resistivity temperature and the magnetic T_c in at least the isotropic perovskite manganites. Moreover, various experimental studies on these manganites have revealed that the microstructure of the Mn-O networks (MnO_6 octahedra) plays a crucial role in the spin-charge dynamics, which is responsible for the magnetic and electrical properties of the compounds. Systematic analyses of the phase diagram of temperature versus tolerance factor (geometrical parameter) have indicated that increasing distortion in the Mn-O-Mn bond angles (or bond lengths) is followed by increasing insulating behavior, decreasing magnetic T_c , and enhanced magnetoresistance effects.^{9,20,21} Alternatively, "charge-ordering" (CO) distortions,²²⁻²⁴ in which the lattice is distorted near a localized hole, are often accompanied by insulating behavior and enhanced magnetoresistance effects. However, the exact role of the Mn-O microstructural networks in the CMR perovskites remains unclear, and the goal of understanding and controlling the CMR in the perovskites is still challenging.

Recently, the effect of the dimensionality of the Mn-O networks on the magnetic and transport properties has been studied with a use of layered perovskite compounds having the general formula $A_{n+1}B_n\text{O}_{3n+1}$. Apart from ABO_3 -type ($n = \infty$) manganites, $A_{n+1}B_n\text{O}_{3n+1}$ -type compounds have layered perovskite structures with two- or quasi-two-dimensional Mn-O networks. Studies of manganese oxide with $n=1$, $\text{La}_{1-x}\text{Sr}_{1+x}\text{MnO}_4$ with a layered perovskite structure (K_2NiF_4 -type) have indicated that the material is a two-dimensional antiferromagnet.^{25,26} Studies on $\text{La}_{2-2x}\text{Sr}_{1+2x}\text{Mn}_2\text{O}_7$ ($x=0.4$) single crystals,²⁷ $\text{La}_{2-2x}\text{Ca}_{1+2x}\text{Mn}_2\text{O}_7$ ($x=0.25$) polycrystalline bulk

samples,²⁸ and ($x=0.3$) thin films²⁹ have shown that manganese oxide with $n=2$ is a two-dimensional ferromagnet which exhibits colossal magnetoresistance effects. These studies and successive studies^{30–32} have found that double perovskite manganites exhibit intriguing features including enhanced MR effects, anisotropic transport in charge carriers, and the possibility of two types of ferromagnetic ordering. In this paper, we report systematic results on the resistivity and magnetization of layered perovskite $\text{La}_{2-2x}\text{Ca}_{1+2x}\text{Mn}_2\text{O}_7$ ($0 \leq x \leq 0.5$) obtained using the bulk and epitaxial thin film samples. We found that the system becomes a metallic ferromagnet for the doping concentrations of $0.22 \leq x \leq 0.5$. With bulk samples in this doping regime, we observe metal-insulator transitions well below the magnetic transition temperature. Although we found the magnetic behavior of thin films with $x=0.3$ to be somewhat different from that of bulk samples with the same concentration, the two critical temperatures were also observed for thin films and coincided well with those of the bulk samples. These observations indicate that the existence of two transition temperatures for magnetic ordering is an intrinsic characteristic of the compound. The magnetoresistance is observed over a wide temperature range from low temperatures to the ferromagnetic ordering temperatures. Based on these results, we present a model of temperature-dependent spin configurations for a layered perovskite ferromagnet with two-dimensional Mn-O networks.

II. EXPERIMENT

The bulk samples we used were prepared by a standard ceramic process. Stoichiometric proportions of La_2O_3 , CaCO_3 , and Mn_2O_3 were mixed, ground, and calcined at 900°C for 20 h in an O_2 atmosphere. The samples were then sintered in the $1400\text{--}1450^\circ\text{C}$ range for 20 h also in an O_2 atmosphere. For film preparation, we used a single-target magnetron sputtering technique. The sputtering technique and conditions we employed were similar to those used for the reproducible production of high-quality high- T_c superconducting oxide thin films.³³ The targets were 70 mm diameter disks with a nominal composition ($\text{La}_{2-2x}\text{Ca}_{1+2x}\text{Mn}_2\text{O}_7$, $x=0.3$); they were prepared by a ceramic process under sintering conditions identical to those used for the bulk samples. Thin films 100–300 nm thick were grown on substrates of MgO (001) and SrTiO_3 (001). Deposition was carried out at a sputtering gas pressure of 76 mTorr Ar and with substrate temperatures in the range $700\text{--}750^\circ\text{C}$. The films were then cooled to room temperature under 10 Torr oxygen. No postdeposition annealing was undertaken. Compositional analyses were performed by energy dispersive x-ray microanalysis (EDX), which indicated that the obtained samples exhibited compositions nearly identical to the nominal one. The properties of the samples remained stable during various heat treatments (annealing in oxygen at $900\text{--}1400^\circ\text{C}$). The crystal structure and the phase purity of the samples were examined by x-ray diffraction with $\text{Cu } K\alpha$ radiation. The electrical resistance and magnetoresistance were measured as a function of temperature (4.2–300 K) and magnetic field (0–1.8 T) by a standard four-point technique. Electrical contacts were made with silver paste. The MR was normalized to the zero-field value, since no saturation was

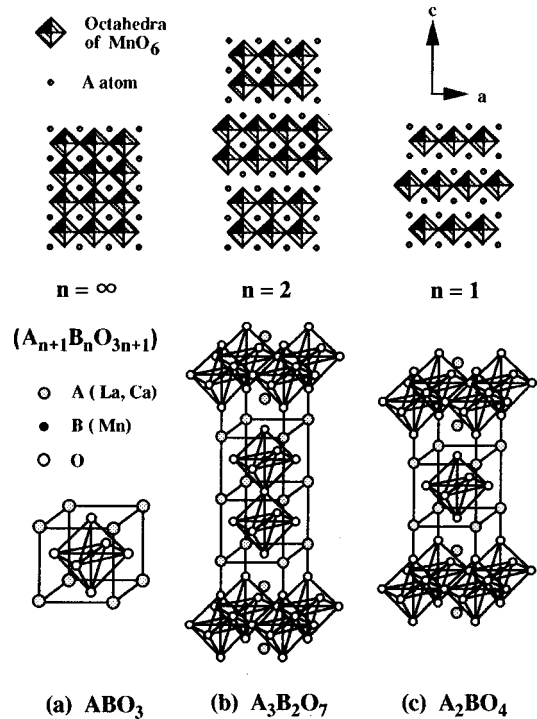


FIG. 1. Schematic views of layer sequences and crystal structures of $A_{n+1}B_nO_{3n+1}$ compounds. (a) ABO_3 compound ($n=\infty$), (b) $A_3B_2O_7$ compound ($n=2$) with a $\text{Sr}_3\text{Ti}_2\text{O}_7$ -type structure, and (c) A_2BO_4 compound ($n=1$) with a K_2NiF_4 -type structure.

achieved in this study. Namely, the MR ratio here is defined as $-\Delta\rho/\rho_0 = -(\rho - \rho_0)/\rho_0$ (where ρ and ρ_0 are the resistivity in an applied magnetic field and the zero field resistivity, respectively). Magnetization was measured on a vibrating sample magnetometer.

III. RESULTS AND DISCUSSION

Our x-ray diffraction study indicated that the $0 \leq x \leq 0.5$ and $x=1.0$ samples were of single phase with a $\text{Sr}_3\text{Ti}_2\text{O}_7$ -type tetragonal perovskite structure ($I4/mmm$).³⁴ By contrast, the $x=0.6$ and $x=0.8$ samples were not of single phase but a mixture with additional impurity phases. Figure 1 shows schematic views of the layer sequences and crystal structures of $A_{n+1}B_nO_{3n+1}$ perovskite compounds. The figure compares views of compounds with $n=\infty$, i.e., ABO_3 , $n=2$, i.e., $A_3B_2O_7$ ($\text{Sr}_3\text{Ti}_2\text{O}_7$ type), and $n=1$, i.e., A_2BO_4 (K_2NiF_4 type) structures. The ABO_3 compound consists of perovskite units with three-dimensional B-O networks. In contrast, $A_3B_2O_7$ and A_2BO_4 structures exhibit two-dimensional B-O networks. The two-dimensional $A_3B_2O_7$ system contains double perovskite layers interleaved with A-O layers, and the two-dimensional A_2BO_4 system has a single perovskite layer interleaved with A-O layers. The good agreement between the calculated and observed relative line intensities obtained for each x value ($0 \leq x \leq 0.5$) ensures that the samples have a high degree of phase purity. In the $\text{La}_{2-2x}\text{Ca}_{1+2x}\text{Mn}_2\text{O}_7$ system with a $\text{Sr}_3\text{Ti}_2\text{O}_7$ -type structure, double perovskite layers are interleaved with La(Ca)O layers, and Mn-O-Mn bonds in the c -axis direction are separated from one another by La(Ca)O layers. In Fig. 2 and Table I, we present the lattice parameter data for the

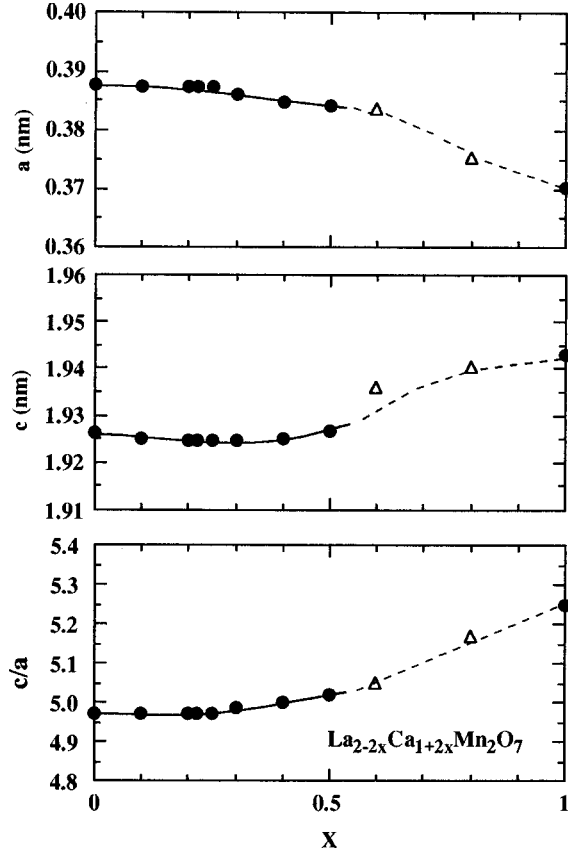


FIG. 2. Lattice parameters of $\text{La}_{2-2x}\text{Ca}_{1+2x}\text{Mn}_2\text{O}_7$ as a function of x . Data for single phase samples with $0 \leq x \leq 0.5$ and $x = 1.0$ are shown as filled circles. Data for samples with $x = 0.6$ and $x = 0.8$, which are denoted as open triangles, are presented only for reference, because these samples are not single phase. The solid and dotted lines are provided only as a guide to the eyes.

$\text{La}_{2-2x}\text{Ca}_{1+2x}\text{Mn}_2\text{O}_7$ system. The general trend is that with increasing x , the a value decreased and the c value decreased. The resultant c/a value increased from 4.970 ($x = 0$) to 5.001 ($x = 0.5$). Diffraction analysis using a four-

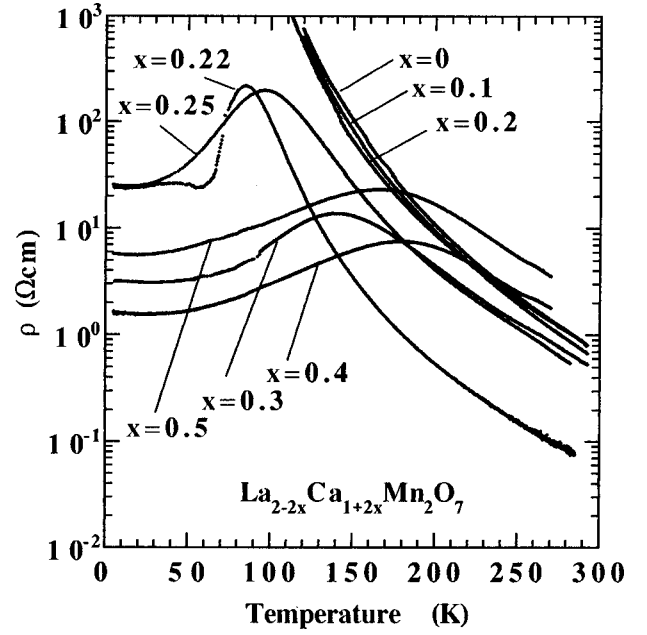


FIG. 3. Temperature dependence of resistivity ρ for $\text{La}_{2-2x}\text{Ca}_{1+2x}\text{Mn}_2\text{O}_7$ samples with $0 \leq x \leq 0.5$.

axis technique showed that the thin films we used in this study had an a -axis normal orientation with the c -axis ordered in the plane and that they consisted of two domains, rotated at 90° to each other in the plane (the so-called mosaic structure). The lattice parameter a_0 for the $x = 0.3$ films on MgO was 0.3868 nm, which is close to the value for bulk with the same concentration.

We used single phase bulk samples of $\text{La}_{2-2x}\text{Ca}_{1+2x}\text{Mn}_2\text{O}_7$ series ($0 \leq x \leq 0.5$) to examine the doping dependence of the transport and magnetic properties. In Fig. 3, we show the temperature dependence of the resistivity ρ for the $\text{La}_{2-2x}\text{Ca}_{1+2x}\text{Mn}_2\text{O}_7$ series ($0 \leq x \leq 0.5$). For $x \leq 0.2$, the ρ - T curve is characteristic of semiconductors or insulators for the whole temperature range we examined. For $x \geq 0.22$, the ρ - T curves exhibit a peak with semiconducting

TABLE I. Summary of physical properties of $\text{La}_{2-2x}\text{Ca}_{1+2x}\text{Mn}_2\text{O}_7$. T_ρ^{\max} , T_{c1} , T_{c2} , and M_s mean the peak temperature in resistivity, the first magnetic ordering temperature (see text), the second magnetic ordering temperature (see text), and the saturated magnetization, respectively.

Sample	Nominal composition x	Lattice constant			T_ρ^{\max} (K)	T_{c1} (K)	T_{c2} (K)	M_s (μ_B/Mn)
		a (nm)	c (nm)	c/a				
Bulk	0	0.3875	1.9261	4.970			160	3.12
Bulk	0.1	0.3872	1.9249	4.971			177	3.20
Bulk	0.2	0.3872	1.9248	4.971			215	3.39
Bulk	0.22	0.3872	1.9248	4.971	88		215	3.58
Bulk	0.25	0.3872	1.9248	4.971	96	85	215	3.59
Bulk	0.3	0.3864	1.9248	4.985	140		251	3.48
Bulk	0.4	0.3849	1.9250	5.001	185		255	2.10
Bulk	0.5	0.3840	1.9267	5.017	173		257	1.55
Bulk	0.6	0.3835	1.9360	5.048				
Bulk	0.8	0.3754	1.9403	5.169				
Bulk	1.0	0.3702	1.9430	5.249				
Film	0.3	0.3868			133	134	250	

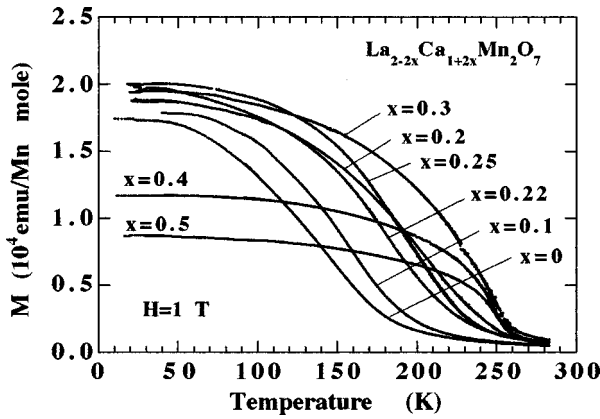


FIG. 4. Temperature variation of bulk magnetization M for samples with $0 \leq x \leq 0.5$. The magnetization was measured in the warming run with a field of 1 T after cooling down to 10 K in a zero field using a vibrating sample magnetometer.

behavior above and metallic behavior below this temperature. Hereafter, the peak temperature in resistivity is designated as T_{ρ}^{\max} . For $x=0.22$, ρ once decreases below T_{ρ}^{\max} , then slightly increases around 60 K, due to some localization effects, and finally decreases from 40 K down to low temperatures. With increments in the nominal hole concentration x from 0.22 up to 0.4, T_{ρ}^{\max} increased from 88 K ($x=0.22$) to 185 K ($x=0.4$) and the resistivity decreased. For $x=0.5$, we observed a slightly reduced T_{ρ}^{\max} of 170 K and a high resistivity. These metal-nonmetal phenomena, which depend on the doping concentrations, are similar to those of the conventional double-exchange ferromagnets such as $\text{La}_{1-x}\text{Ca}_x\text{MnO}_3$.

Figure 4 displays the temperature dependence of magnetization M for bulk samples with $0 \leq x \leq 0.5$. The magnetization was measured in the warming run with a field of 1 T after cooling down to 10 K in a zero field. The bulk magnetic transition temperatures T_c were determined from the M - T curves by the conventional M^2 - T method. As x increases, the bulk T_c values increase from 160 K ($x=0$) and 215 K ($x=0.22$) to 257 K ($x=0.5$). When comparing the T_c values with the T_{ρ}^{\max} values for corresponding doping concentrations, the T_c values were about 100 K higher than the T_{ρ}^{\max} values. Namely, for the $\text{La}_{2-2x}\text{Ca}_{1+2x}\text{Mn}_2\text{O}_7$ bulk samples, no coincidence can be seen between the metal-insulator transition and the magnetic transition, as commonly observed for ABO_3 -type ferromagnets with three dimensional Mn-O-Mn networks. Figure 5 plots the change in the magnitude of the magnetic moments, which is determined from the saturated magnetization at low temperatures, as a function of x . As x increases from $x=0$, the M_s first increases from $3.12\mu_B/\text{Mn}$ ($x=0$) to $3.58\mu_B/\text{Mn}$ ($x=0.22$), reaching a maximum value of $3.59\mu_B/\text{Mn}$ ($x=0.25$), and then decreases steeply to $1.55\mu_B/\text{Mn}$ ($x=0.5$). The M_s value of $3.59\mu_B/\text{Mn}$ ($x=0.25$) is in good agreement with the expected value of $3.75\mu_B/\text{Mn}$ for the average oxidation state of 3.25 for Mn cations, indicating that the $x=0.25$ compound possesses a fully ordered spin alignment. A slightly reduced magnetic moment in the lower x range may suggest the canted ferromagnetic spin arrangement, as is the case with canted ferromagnetic insulators³⁵ in the $\text{La}_{1-x}\text{Sr}_x\text{MnO}_3$ system with low

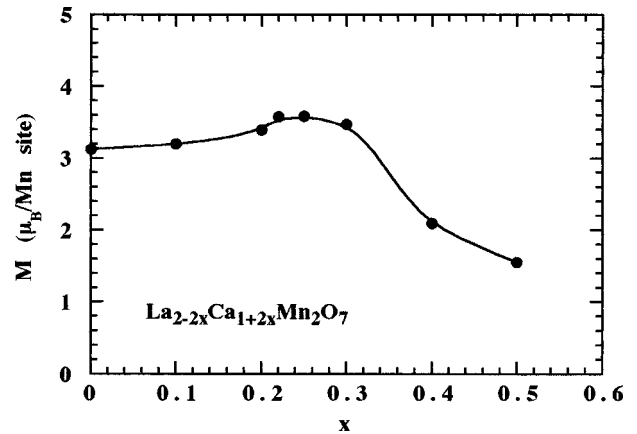


FIG. 5. Change in the magnitude of the magnetic moments as a function of x for $\text{La}_{2-2x}\text{Ca}_{1+2x}\text{Mn}_2\text{O}_7$.

doping concentrations. The large reduction in the magnetic moment in the higher x range could be ascribed to the contribution of the antiferromagnetic interaction between Mn^{4+} cations.

The temperature dependence of the MR ratio $-\Delta\rho/\rho_0$ (at $\mu_0H=1.8$ T) of $\text{La}_{2-2x}\text{Ca}_{1+2x}\text{Mn}_2\text{O}_7$ for concentrations of $x=0.22, 0.25, 0.3, 0.4$, and 0.5 is shown in Fig. 6. In the figure, arrows indicate the resistivity cusp temperature T_{ρ}^{\max} and the magnetic T_c determined by magnetization measurement. It can be seen that the MR effect of these samples exhibits a complicated temperature dependence over a wide temperature range. As regards the MR effect, three temperature regions can be identified; a region around T_c , a region around T_{ρ}^{\max} , and a region well below T_{ρ}^{\max} . The first small peak for all the samples can be observed at temperatures around the bulk magnetic T_c , and a second peak with a larger magnitude is present in the region around T_{ρ}^{\max} . This temperature-dependent MR behavior near and above T_{ρ}^{\max} is suggestive of the occurrence of such a type of transition that the double-exchange model would predict. Moreover, it is noteworthy that a large MR is also observed in the region well below T_{ρ}^{\max} and the temperature variation is different for each sample. For $x=0.22$, a positive MR is observed in the 50–70 K range, which is close to the resistivity minimum seen in Fig. 3. In Fig. 7, we plot the x dependence of the MR ratio $-\Delta\rho/\rho_0$ (1.8 T) at $\sim T_{\rho}^{\max}$ and the low temperature for the bulk samples. Here, the MR ratio at $\sim T_{\rho}^{\max}$ and the low temperature is taken from the local maximum of the MR ratio near T_{ρ}^{\max} and the low temperature in Fig. 6, respectively. It is evident that the x dependence is quite different for the MR ratio at the low temperature and $\sim T_{\rho}^{\max}$, possibly implying that the mechanism of the MR effects is not the same. The MR (peak) value near T_{ρ}^{\max} is rather high in the vicinity ($x=0.22$ – 0.25) of the compositional boundary of the metal-insulator transition, and decreases steeply with increasing x . The observed doping dependence of the MR value at T_{ρ}^{\max} is similar to that of a conventional double-exchange ferromagnet¹⁹ such as $\text{La}_{1-x}\text{Ca}_x\text{MnO}_3$, which is interpreted in terms of the doping-dependent effective coupling strength, J/W , between the mobile carriers and the localized spins, where J is the on-site Hund coupling, and W is the electronic bandwidth.³⁶ The origin of the low-

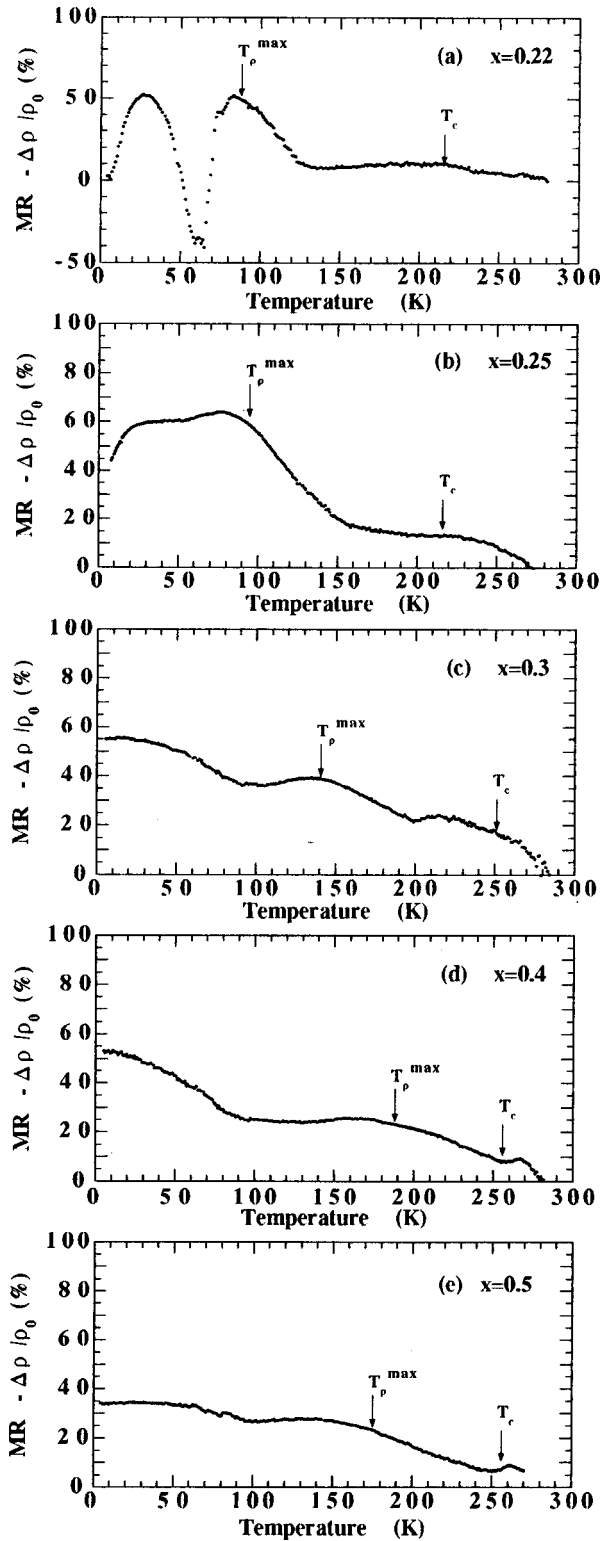


FIG. 6. The temperature dependences of the MR ratio $-\Delta\rho/\rho_0$ of $\text{La}_{2-2x}\text{Ca}_{1+2x}\text{Mn}_2\text{O}_7$ for $x=0.22$ (a), $x=0.25$ (b), $x=0.3$ (c), $x=0.4$ (d), and $x=0.5$ (e). Arrows indicate the cusp temperatures in resistivity T_p^{\max} , and the magnetic transition temperatures T_c . The MR ratio is measured at an applied field of 1.8 T.

temperature MR of the bulk samples is discussed later.

The observed systematic change in the electrical and magnetic properties of bulk samples with various doping concentrations is, as a whole, similar to those of cubic

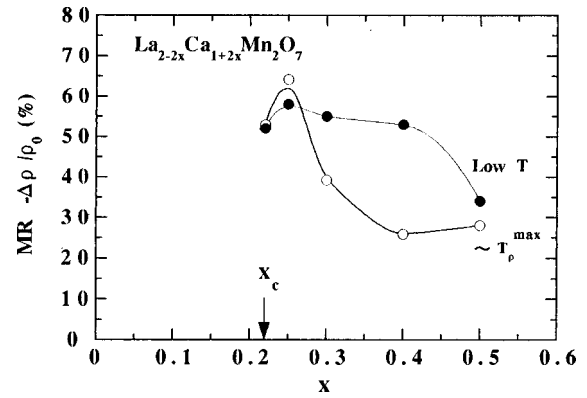


FIG. 7. The x dependence of MR ratio $-\Delta\rho/\rho_0$ at $\sim T_p^{\max}$ and low temperature for the bulk samples. Here, the MR ratio at $\sim T_p^{\max}$ (shown in open circles) and the low temperature (shown in closed circles) is taken from the local maximum of MR ratio (in Fig. 6) near T_p^{\max} and the low temperature, respectively. The arrow indicates the compositional boundary of the metal-insulator transition. The solid lines are eye guides.

(or pseudocubic) perovskite manganites with isotropic Mn-O networks. This suggests that the fundamental mechanism of the metallic ferromagnetism in double-perovskite $\text{La}_{2-2x}\text{Ca}_{1+2x}\text{Mn}_2\text{O}_7$ can be interpreted primarily within the framework of the double-exchange theory. Then, the most striking observation in the bulk samples of double-perovskite manganites is the large deviation between the metal-insulator transition and the magnetic transition, while a good correlation has been commonly observed between the T_p^{\max} and the T_c for the cubic perovskite manganites. Here, it is important to mention an extrinsic effect, which could result in a large deviation in T_p^{\max} and T_c , such as the grain size effect^{37,38} reported for bulk samples of cubic perovskite. It was found that samples with a small grain size less than $\sim 0.5 \mu\text{m}$ exhibited a T_p^{\max} far (100 K) below T_c , whereas for samples with a grain size larger than $\sim 1 \mu\text{m}$ there is good agreement between T_p^{\max} and T_c . Examination with a scanning electron microscope indicated that the $\text{La}_{2-2x}\text{Ca}_{1+2x}\text{Mn}_2\text{O}_7$ samples had an average grain size of larger than $2 \mu\text{m}$. Therefore, this grain size effect can be ruled out as the origin of the present observation. This observation can be interpreted in terms of the existence of two types of ferromagnetic ordering caused by the anisotropic carrier transport and exchange interaction in the compound. We assume that, at around the cusp temperature, the electrical properties of the bulk samples are dominated by less conductive transport along the out-of-plane direction, which is due to a weaker exchange interaction. By contrast, the magnetic transition of the bulk materials would be governed by the strong in-plane exchange interaction. Thus, T_p^{\max} is observed far below the T_c of the bulk samples. To verify the existence of two types of ferromagnetic ordering in the compounds, we examined the related properties of the epitaxial film samples and compared them with those of the bulk samples.

Figure 8 compares the temperature dependence of resistivity ρ (a), magnetization M and inverse susceptibility $1/\chi$ (b), and MR ratio $-\Delta\rho/\rho_0$ (c) for bulk and a -axis film samples of $\text{La}_{2-2x}\text{Ca}_{1+2x}\text{Mn}_2\text{O}_7$ ($x=0.3$). There is a cusp in the ρ - T curves both for samples with metallic behavior be-

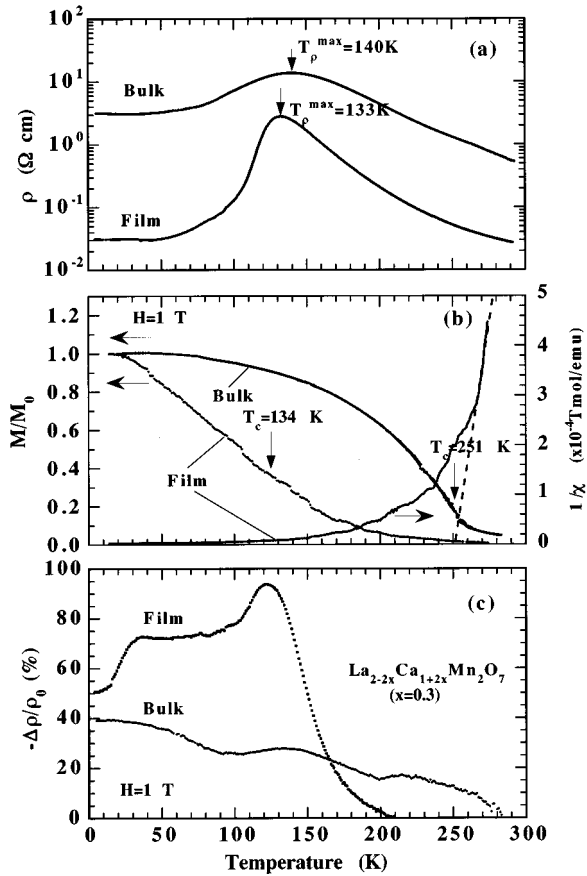


FIG. 8. Resistivity ρ (a), magnetization M and inverse susceptibility $1/\chi$ (b), and MR ratio of $-\Delta\rho/\rho_0$ (c) for bulk and thin film samples of $\text{La}_{2-2x}\text{Ca}_{1+2x}\text{Mn}_2\text{O}_7$ ($x=0.3$) as a function of temperature. The MR ratio $-\Delta\rho/\rho_0$ and the magnetization are measured under an applied field of 1 T. Arrows indicate the cusp temperatures in resistivity T_{ρ}^{\max} , and the magnetic transition temperatures T_c .

low and semiconducting behavior above this temperature. The T_{ρ}^{\max} value of 133 K of the thin film is in good agreement with that (140 K) of the bulk sample, which ensures stoichiometry, that is, an appropriate doping concentration. The thin film resistivities ρ were much smaller (by one order of magnitude at room temperature and around T_{ρ}^{\max} and by two orders of magnitude at 4.2 K) than those of the bulk sample. This is attributable to the great reduction in grain-boundary scattering in the epitaxial films. As mentioned above, the T_c of the bulk samples of the compound was always much higher than their T_{ρ}^{\max} , and for $x=0.3$ the T_c and T_{ρ}^{\max} were 251 and 140 K, respectively. In contrast, the thin film exhibited a T_c of 134 K, derived from M^2 - T plotting, which is in fairly good agreement with their T_{ρ}^{\max} of 133 K. However, at temperatures much higher than T_c (134 K), there is still definite magnetization, possibly reflecting two-dimensional spin ordering, as shown in Fig. 8(b). From the $1/\chi$ - T curve for thin film with $x=0.3$, shown in Fig. 8(b), it is evident that $1/\chi$ exhibits a linear temperature dependence above ~ 260 K, and the temperature extrapolated from the higher-temperature Curie-Weiss plot, as shown by the dotted line in Fig. 8(b), is 250 K, and this is very close to the T_c of the bulk sample (251 K) with the same doping concentration. It should also be mentioned that in the M - T measurements

for bulk samples in a low magnetic field (1 mT), a feature was observed at around their T_{ρ}^{\max} . Thus, the M - T behavior depending on the sample form would reflect an anisotropic nature of the double perovskite ferromagnet. The temperature dependence of the MR ratio $-\Delta\rho/\rho_0$ ($H=1$ T) for thin film and bulk samples is compared in Fig. 8(c). There are clear differences between the temperature-dependent MR behavior of the thin film and that of the bulk. These differences can be summarized in three typical aspects, that is, MR at T_{ρ}^{\max} , MR at temperatures above ~ 200 K, and MR at temperatures below ~ 100 K. With the thin film, the largest MR effect was observed at around T_{ρ}^{\max} (133 K) and the maximum MR ratio was 93%. In the MR- T curve for the bulk, at around T_{ρ}^{\max} (140 K) we observed a second maximum with a $-\Delta\rho/\rho_0$ of 30%. With regard to the MR effect at temperatures above ~ 200 K, the bulk sample exhibited a small but significant MR effect up to room temperature. In contrast, the thin film showed no MR effect in this temperature range. This temperature-dependent MR behavior of the thin film and bulk samples is closely associated with their respective M - T behavior. The present bulk data as well as the thin film data provide strong evidence that the existence of two transition temperatures for magnetic ordering is behavior which is intrinsic to the compound.

To understand the spin-charge coupling phenomena in perovskites with two-dimensional Mn-O networks, it is essential to adopt the double-exchange model by taking account of their anisotropic nature. In this model, the transfer integral t_{ij} between neighboring Mn sites is expressed as $t_{ij}=b_{ij}\cos(\theta_{ij}/2)$, where b_{ij} is the transfer matrix element, which describes electron hopping between Mn sites, and θ_{ij} is the relative angle of the local spins. The matrix element b_{ij} would govern the coupling between the mobile electrons and the localized electrons, hence the ferromagnetic transition temperature and the electronic conductivity. It is plausible that, in the layered perovskite, the motion of doped holes and hence the exchange interaction would be anisotropic in the a - b axis (in-plane) and c -axis (out-of-plane) directions. The anisotropic exchange interaction could be the reason for the two transition temperatures for magnetic ordering, since the magnetic critical temperature is usually proportional to the strength of the exchange interaction. The Mn-Mn interaction due to the series of Mn-O-Mn bonds in the in-plane direction is stronger than the Mn-Mn interaction resulting from the series of alternating Mn-O-Mn and Mn-O-O-Mn bonds in the out-of-plane direction, when we consider that the Mn-Mn interaction due to the Mn-O-O-Mn bonds is an antiferromagnetic exchange interaction, as suggested by the results for $\text{La}_{1-x}\text{Sr}_{1+x}\text{MnO}_4$.^{25,26} So, we believe that the in-plane exchange interaction is stronger than the out-of-plane exchange interaction, and that the probability of electron hopping (hole transfer) in the in-plane direction is much higher than that in the out-of-plane direction. Different parameters b_{ij} can be assumed for the electron hopping in the in-plane and out-of-plane directions, b_{ab} and b_c , respectively, with $b_{ab}>b_c$. Therefore, the lower critical temperature we observed results from the out-of-plane exchange interaction, and the higher critical temperature results from the in-plane exchange interaction. Table I lists data on these critical temperatures (T_{ρ}^{\max} , T_{c1} , and T_{c2}) for the bulk and thin film samples. For the

bulk samples, the lower ordering temperatures, designated by T_{c1} , are determined from the M - T curve in a magnetic field of 1 mT, and the higher ordering temperatures, designated by T_{c2} , are obtained from the M - T curve in a magnetic field of 1 T. For the thin film, T_{c1} is determined from the M - T curve in a magnetic field of 1 T, and T_{c2} is obtained from the high-temperature Curie-Weiss plot in a magnetic field of 1 T. It should be noted that for both bulk and thin films T_{ρ}^{\max} is very close to T_{c1} . At around T_{c1} ($\sim T_{\rho}^{\max}$) and T_{c2} , the behavior of carrier motion and spin ordering is considered to be as follows. At around T_{c1} ($\sim T_{\rho}^{\max}$), two-dimensional spin fluctuation occurs in the out-of-plane direction, while spin ordering is still preserved in the in-plane direction. Thus, the resultant resistivity maximum is observable for polycrystalline bulk and a -axis thin films, since the electrical properties of both samples are dominated by the less mobile carrier transport in the out-of-plane direction. An applied magnetic field can easily restore the two-dimensional spin order and reduce the spin scattering of the conduction electrons, thus giving rise to large MR effects at around T_{c1} . By contrast, at around T_{c2} the in-plane exchange interaction contributes to the magnetic and electrical properties, and there is also a large spin fluctuation in the in-plane direction. Two-dimensional spin ordering still remains in the compound above T_{c1} up to T_{c2} . Small anomalies in the electrical properties at around the higher critical temperature, namely, smaller MR effects and the negligible structure in the resistivity data, can possibly be attributed to the contribution of thermally activated conduction with significantly reduced resistivity in the out-of-plane direction.

We could deduce the magnetic phase diagram based on the bulk data for the double-octahedral perovskite $\text{La}_{2-2x}\text{Ca}_{1+2x}\text{Mn}_2\text{O}_7$ and this is shown in Fig. 9. The low temperature state is a (canted) ferromagnetic insulator for $0 \leq x \leq 0.2$, and a ferromagnetic metal appears for $x \geq 0.22$. For a low doping region with $x < 0.2$, we observed only the transition between a ferromagnetic insulator (FI) and a paramagnetic insulator (PI). It is seen that for $0.22 \leq x \leq 0.5$ the bulk materials behave such that they undergo two transitions from a paramagnetic insulator (PI) to a ferromagnetic insulator (FI) and finally to a ferromagnetic metal (FM) with decreasing temperature. It must be noted that the FI state in Fig. 9 should exhibit a two-dimensional ferromagnetic arrangement and an anisotropic carrier motion with intrinsically insulatorlike transport in the out-of-plane direction and metallic transport in the in-plane direction. The phase diagram for a broad range of temperatures and concentrations of the $\text{La}_{1-x}\text{Ca}_x\text{MnO}_3$ system has been reported by Schiffer *et al.*⁸ A comparison of the phase diagrams of the $\text{La}_{2-2x}\text{Ca}_{1+2x}\text{Mn}_2\text{O}_7$ and $\text{La}_{1-x}\text{Ca}_x\text{MnO}_3$ systems may provide useful information about the characteristics of double-perovskite and isotropic-perovskite ferromagnetic manganites. The most distinct difference between the two systems is the regime under which a ferromagnetic insulating state exists. In the $\text{La}_{1-x}\text{Ca}_x\text{MnO}_3$ system, this state exists only for a low (nominal) hole-concentration range. By contrast, in the $\text{La}_{2-2x}\text{Ca}_{1+2x}\text{Mn}_2\text{O}_7$ system, the regime of the ferromagnetic insulating state extends over the wide range of hole concentrations ($0 \leq x \leq 0.5$) and temperatures examined in this study. Moreover, the ferromagnetic insulating phase ap-

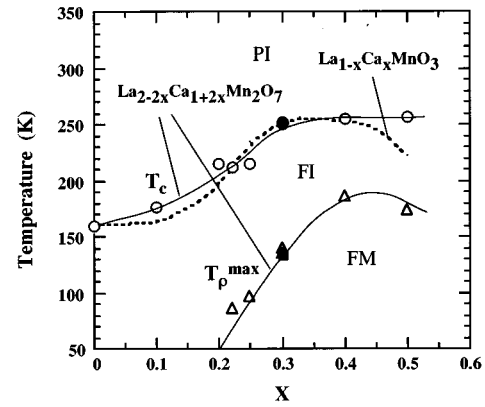


FIG. 9. Magnetic phase diagram of $\text{La}_{2-2x}\text{Ca}_{1+2x}\text{Mn}_2\text{O}_7$, based on the present bulk data. The abbreviations mean paramagnetic insulator (PI), ferromagnetic insulator (FI), and ferromagnetic metal (FM). The triangles denote the peak temperature in resistivity T_{ρ}^{\max} . The circles denote the magnetic transition temperature T_c . The solid lines through the data for $\text{La}_{2-2x}\text{Ca}_{1+2x}\text{Mn}_2\text{O}_7$ are eye guides. For comparison, previously reported data⁸ for the $\text{La}_{1-x}\text{Ca}_x\text{MnO}_3$ system are shown by dotted lines.

pears between the ferromagnetic metal and paramagnetic insulator phases in the $0.22 \leq x \leq 0.5$ range. Another important finding is that the doping dependence of T_{c2} in the $\text{La}_{2-2x}\text{Ca}_{1+2x}\text{Mn}_2\text{O}_7$ system is very close to that of T_c (and therefore T_{ρ}^{\max}) in the $\text{La}_{1-x}\text{Ca}_x\text{MnO}_3$ system, which contains only one type of Mn-Mn interaction. This agreement also provides strong evidence that the T_{c2} value of $\text{La}_{2-2x}\text{Ca}_{1+2x}\text{Mn}_2\text{O}_7$ is determined by the in-plane exchange interaction.

On the basis of the above discussion, we propose the model of temperature-dependent spin alignment for the double-layer perovskite manganite shown in Fig. 10. This figure also shows, for convenience, the magnetic phase diagram and the schematic views of layer sequences for the compound. This model is primarily considered to describe the behavior of a metallic ferromagnet of double perovskite manganite with a doping concentration of $x \sim 0.3$. We adopt four temperature ranges: (a) $T \ll T_{c1}$, (b) $T \leq T_{c1}$, (c) $T_{c1} < T < T_{c2}$, and (d) $T > T_{c2}$. At $T \ll T_{c1}$, there is ferromagnetic spin ordering within a double MnO_2 layer and between neighboring double MnO_2 layers. At $T \leq T_{c1}$, there is increased spin fluctuation in the out-of-plane direction between neighboring double MnO_2 layers, whereas spin ordering in the in-plane direction is still preserved. At $T_{c1} < T < T_{c2}$, there is an appreciable amount of two-dimensional spin fluctuation in the out-of-plane direction between neighboring double MnO_2 layers. Finally, at $T > T_{c2}$, spin ordering completely disappears. The most notable feature in double-layer perovskite manganite is the behavior in the $T_{c1} < T < T_{c2}$ range, where there is two-dimensional ferromagnetic alignment. In this temperature range, the observed transport and magnetic properties are highly dependent on the sample form (e.g., polycrystals or single crystals), because of the two-dimensional ferromagnetic arrangement and the anisotropic carrier motion with intrinsically insulatorlike transport in the out-of-plane direction and metallic transport in the in-plane direction. This model can reasonably explain a recent observation²³ in single crystal $\text{La}_{2-2x}\text{Sr}_{1+2x}\text{Mn}_2\text{O}_7$ (x

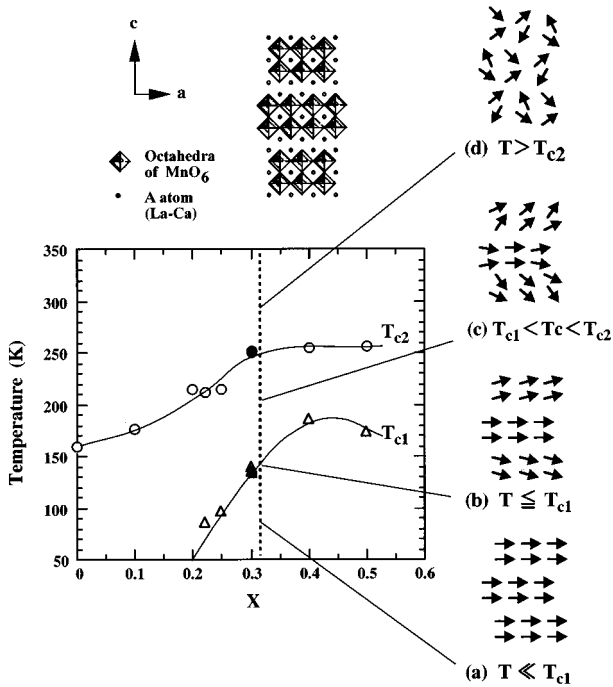


FIG. 10. Proposed model of temperature-dependent spin alignment for the double-perovskite ferromagnet $\text{La}_{2-2x}\text{Ca}_{1+2x}\text{Mn}_2\text{O}_7$, together with the magnetic phase diagram, and schematic views of the layer sequences for the compound. The arrows denote the spin directions of Mn cations. The solid lines are eye guides.

$=0.3$) that the T_ρ^{\max} values themselves depend on the crystal directions. Using the present simple model of spin alignment, we are also able to explain at least qualitatively the magnetoresistance effect observed over the wide temperature range, except for the low-temperature MR in the $T \ll T_{c1}$ range. However, the doping concentrations of the charge carriers are also likely to affect the detailed spin arrangement, as is well known for isotropiclike perovskite manganites. Even the degree of the dimensionality in layered perovskite manganites is also likely to affect the detailed spin arrangement. Further investigations are necessary to elucidate these issues.

The magnitude of the MR effect in $\text{La}_{2-2x}\text{Ca}_{1+2x}\text{Mn}_2\text{O}_7$ has been enhanced for almost the whole temperature region by comparison with the CMR perovskites with three-dimensional Mn-O networks. The origin of the enhanced MR properties in this compound can be ascribed to anisotropic Mn-O networks with reduced dimensions. The simple explanation is that the two dimensionality of the Mn-O networks causes a reduction in the effective transfer interaction of the e_g carriers, which gives rise to enhanced effective coupling between the local spin and the charge carrier via strong intratomic ferromagnetic (Hund) coupling. However, an additional and more important factor, we suggest, is the anisotropic exchange interaction in this compound. The overall Mn-Mn exchange interaction in the out-of-plane direction, which is due to the series of alternating Mn-O-Mn and Mn-O-O-Mn bonds, is essentially weaker than the double ex-

change interaction due to the series of Mn-O-Mn bonds in the in-plane-direction. Near the lower critical temperature corresponding to the cusp temperature T_ρ^{\max} , there is two-dimensional spin fluctuation in the out-of-plane direction, while ferromagnetic spin ordering is preserved in the in-plane-direction. An external magnetic field could easily restore the two-dimensional spin order and therefore enhance the transfer of the conduction electrons, thus giving rise to large MR effects with a relatively lower magnetic field in this temperature range. The enhanced MR effect in the layered perovskite manganese ferromagnet is most consistent with an anisotropic exchange interaction in combination with a very narrow one-electron bandwidth. Moreover, it should be noted that, in the low temperature range well below T_ρ^{\max} , there is an appreciable MR effect for both the bulk and thin film samples. The resistivity versus applied magnetic field curve data³⁹ on polycrystalline bulk and thin films show that the origin of the low-temperature MR effect in the double-layer perovskite manganite is different for polycrystalline bulk and thin films. The low-temperature MR for polycrystalline bulk is mainly due to the magnetic-domain-based mechanism coupled with either spin scattering at grain boundaries⁸ or spin-polarized intergrain tunneling.⁴⁰ The low-temperature MR for *a*-axis thin films is possibly due to the spin-polarized tunneling effects^{41,42} in the stacked layers between a metallic $(\text{MnO}_2)_2$ layer and an insulating $\text{La}(\text{Ca})_2\text{O}_2$ layer, which is reminiscent of the intrinsic Josephson tunneling effects⁴³ in high- T_c copper oxide perovskites. Although it is reasonable to assume a domain-based mechanism to account for the spin-polarized tunneling effects, the contribution of the exact configuration of the two-dimensional spin ordering in the double perovskite manganites should be taken into consideration. Further studies are needed to clarify the role of two-dimensional spin ordering as regards the possible formation of Jahn-Teller polarons and the CMR phenomena in manganese perovskite ferromagnet.

IV. SUMMARY

We have used bulk and thin film samples of the double perovskite $\text{La}_{2-2x}\text{Ca}_{1+2x}\text{Mn}_2\text{O}_7$ series with various doping concentrations x to investigate the transport and magnetic properties associated with metal-insulator and magnetic transitions. The results provide clear evidence for the existence of two distinct types of ferromagnetic ordering, which possibly results from an anisotropic exchange interaction, in the $0.22 \leq x \leq 0.5$ dopant regime. It can be seen that bulk materials with these doping concentrations behave such that they undergo two transitions from a paramagnetic insulator to a ferromagnetic insulator and finally to a ferromagnetic metal with decreasing temperature. Magnetoresistance was observed over a wide temperature range from low temperatures to the ferromagnetic ordering temperatures. Based on these results, we presented a model of the temperature-dependent spin configurations for a layered perovskite ferromagnet with two-dimensional Mn-O networks, suggesting that there is two-dimensional ferromagnetic alignment at temperatures between the two ordering temperatures.

- ¹ C. W. Searle and S. T. Wang, *Can. J. Phys.* **47**, 2023 (1969).
- ² R. M. Kusters, J. Singleton, D. A. Keen, R. McGreevy, and W. Hayes, *Physica B* **155**, 362 (1989).
- ³ R. von Helmolt, J. Wecker, B. Holzapfel, L. Schultz, and K. Samwer, *Phys. Rev. Lett.* **71**, 2331 (1993).
- ⁴ K. Chahara, T. Ohno, M. Kasai, and Y. Kozono, *Appl. Phys. Lett.* **63**, 1990 (1993).
- ⁵ Y. Tokura, A. Urushibara, Y. Moritomo, T. Arima, A. Asamitsu, G. Kido, and N. Furukawa, *J. Phys. Soc. Jpn.* **63**, 3931 (1994).
- ⁶ H. L. Ju, C. Kwon, Qi Li, R. L. Greene, and T. Venkatesan, *Appl. Phys. Lett.* **65**, 2117 (1994).
- ⁷ S. Jin, H. M. O'Bryan, T. H. Tiefel, M. McCormack, and W. W. Rhodes, *Appl. Phys. Lett.* **66**, 382 (1995).
- ⁸ P. Schiffer, A. P. Ramirez, W. Bao, and S. W. Cheong, *Phys. Rev. Lett.* **75**, 3336 (1995).
- ⁹ H. Y. Hwang, S. W. Cheong, P. G. Radaelli, M. Marezio, and B. Batlogg, *Phys. Rev. Lett.* **75**, 914 (1996).
- ¹⁰ C. Zener, *Phys. Rev.* **82**, 403 (1951).
- ¹¹ P. W. Anderson and H. Hasegawa, *Phys. Rev.* **100**, 675 (1955).
- ¹² P. G. de Gennes, *Phys. Rev.* **118**, 141 (1960).
- ¹³ A. J. Millis, P. B. Littlewood, and B. I. Shraiman, *Phys. Rev. Lett.* **74**, 5144 (1995).
- ¹⁴ H. Roder, J. Zang, and A. R. Bishop, *Phys. Rev. Lett.* **76**, 1356 (1996).
- ¹⁵ G. Zhao, K. Conder, H. Keller, and K. A. Muller, *Nature (London)* **381**, 676 (1996).
- ¹⁶ A. Shengelaya, G. Zhao, H. Keller, and K. A. Muller, *Phys. Rev. Lett.* **76**, 5296 (1996).
- ¹⁷ A. P. Ramirez, P. Schiffer, S. W. Cheong, C. H. Chen, W. Bao, T. T. Palstra, P. L. Gammel, D. J. Bishop, and B. Muller, *Phys. Rev. Lett.* **76**, 3188 (1996).
- ¹⁸ S. G. Kaplan, M. Quijada, H. D. Drew, D. B. Tanner, G. C. Xiong, R. Ramesh, C. Kwon, and T. Venkatesan, *Phys. Rev. Lett.* **77**, 2091 (1996).
- ¹⁹ A. Urushibara, Y. Moritomo, T. Arima, A. Asamitsu, G. Kido, and Y. Tokura, *Phys. Rev. B* **51**, 14 103 (1995).
- ²⁰ R. G. Radaelli, M. Marazio, H. Y. Hwang, S. W. Cheong, and B. Batlogg, *Phys. Rev. B* **54**, 8992 (1996).
- ²¹ J. M. D. Teresa, M. R. Ibarra, J. Garcia, J. Blasco, C. Ritter, P. A. Algarabel, C. Marquina, and A. D. Moral, *Phys. Rev. Lett.* **76**, 3392 (1996).
- ²² H. Yoshizawa, H. Kuwano, Y. Tomioka, and Y. Tokura, *Phys. Rev. B* **52**, R13 145 (1995).
- ²³ Y. Tomioka, A. Asamitsu, Y. Moritomo, H. Kuwahara, and Y. Tokura, *Phys. Rev. Lett.* **74**, 5108 (1995).
- ²⁴ M. R. Lees, J. Barratt, G. Balakrishnan, D. M. Paul, and M. Yethiraj, *Phys. Rev. B* **52**, R14303 (1995).
- ²⁵ C. N. R. Rao, P. Ganguly, K. K. Singh, and R. A. Mohan Ram, *J. Solid State Chem.* **72**, 14 (1988).
- ²⁶ Y. Moritomo, Y. Tomioka, A. Asamitsu, Y. Tokura, and Y. Matsui, *Phys. Rev. B* **51**, 3297 (1995).
- ²⁷ Y. Moritomo, Y. Tomioka, A. Asamitsu, Y. Tokura, and Y. Matsui, *Nature (London)* **380**, 141 (1996).
- ²⁸ H. Asano, J. Hayakawa, and M. Matsui, *Appl. Phys. Lett.* **68**, 3638 (1996).
- ²⁹ H. Asano, J. Hayakawa, and M. Matsui, *Jpn. J. Appl. Phys. 2, Lett.* **36**, L104 (1997).
- ³⁰ T. Kimura, Y. Tomioka, H. Kuwahara, A. Asamitsu, M. Tamura, and Y. Tokura, *Science* **274**, 1698 (1996).
- ³¹ P. D. Battle, M. A. Green, N. S. Laskey, J. E. Millburn, M. J. Rosseinsky, S. P. Sullivan, and J. F. Vente, *Phys. Rev. B* **54**, 15 967 (1996).
- ³² R. Suryanarayanan, I. Zelenay, and J. Berthon, *Mater. Res. Bull.* **32**, 595 (1997).
- ³³ H. Asano, H. Yonezawa, M. Asahi, and O. Michikami, *IEEE Trans. Magn.* **27**, 844 (1991).
- ³⁴ S. N. Ruddlesden and P. Popper, *Acta Crystallogr.* **54**, 11 (1958).
- ³⁵ D. N. Argyrio, J. F. Mitchell, C. D. Potter, D. G. Hinks, J. D. Jorgensen, and S. D. Bader, *Phys. Rev. Lett.* **76**, 3826 (1996).
- ³⁶ N. Furukawa, *J. Phys. Soc. Jpn.* **63**, 3214 (1994).
- ³⁷ R. Mahesh, R. Mahendiran, A. K. Raychaudhuri, and C. N. R. Rao, *Appl. Phys. Lett.* **68**, 2291 (1996).
- ³⁸ R. Mahendiran, R. Mahesh, A. K. Raychaudhuri, and C. N. R. Rao, *Solid State Commun.* **99**, 149 (1996).
- ³⁹ H. Asano, J. Hayakawa, and M. Matsui, *Appl. Phys. Lett.* **70**, 2303 (1997).
- ⁴⁰ H. Y. Hwang, S. W. Cheong, N. P. Ong, and B. Batlogg, *Phys. Rev. Lett.* **77**, 2041 (1996).
- ⁴¹ T. Miyazaki and N. Tezuka, *J. Magn. Magn. Mater.* **151**, 403 (1995).
- ⁴² J. S. Moodera, L. R. Kinder, T. M. Wong, and R. Meservey, *Phys. Rev. Lett.* **74**, 3273 (1995).
- ⁴³ R. Kleiner, F. Steinmeyer, G. Kunkel, and P. Muller, *Phys. Rev. Lett.* **68**, 2394 (1992).